

# A Survey on Infrared Image & Video Sets

Kevser Irem Danaci<sup>1\*</sup> and Erdem Akagunduz<sup>2</sup>

<sup>1</sup>Department of Electrical Engineering, Sivas University of Science And Technology, Turkey.

<sup>2\*</sup>The Graduate School of Informatics, Middle East Technical University, Turkey.

[kiremdanaci@sivas.edu.tr](mailto:kiremdanaci@sivas.edu.tr); [akaerdem@metu.edu.tr](mailto:akaerdem@metu.edu.tr);

## Abstract

In this survey, we compile a list of publicly available infrared image and video sets for artificial intelligence and computer vision researchers. We mainly focus on IR image and video sets which are collected and labelled for computer vision applications such as object detection, object segmentation, classification, and motion detection. We categorize 92 different publicly available or private sets according to their sensor types, image resolution, and scale. We describe each and every set in detail regarding their collection purpose, operation environment, optical system properties, and area of application. We also cover a general overview of fundamental concepts that relate to IR imagery, such as IR radiation, IR detectors, IR optics and application fields. We analyse the statistical significance of the entire corpus from different perspectives. We believe that this survey will be a guideline for computer vision and artificial intelligence researchers that would want to delve into working with the spectra beyond the visible domain.

**Keywords:** Infrared Image & Video Sets, Infrared Imagery, Survey

## 1 Introduction

Data, becoming the foundation for the field of artificial intelligence, is the defining element of science in the new century. Machine learning techniques are becoming more sophisticated every year, are now capable of processing bigger data than humanity has ever imagined or possessed. Specifically, in the field of computer vision, the effect of large-scale image and video sets on certain machine learning tasks is so dramatic that deep neural networks perform better than or are on par with humans on especially good quality images [27]. As of today, the amount of available labelled visual data for various computer vision tasks (such as image classification, segmentation, detection, tracking, etc.) reaches billions [104] of high-quality images that are worldwide available for use by scientists and engineers.

Publicly accessible visual data can be found in different modalities. Although the available data is overwhelmingly composed of the visible band, or in other words, “RGB” images; public access to images of other modalities, such as multi/hyperspectral, magnetic resonance (MR), computerized tomography (CT), synthetic aperture radar (SAR), depth just to name a few, is also possible. One of the relatively less public imaging modalities is the infrared (IR) imagery, which corresponds to images constructed with the radiation of an invisible portion of the electromagnetic spectrum, known as the IR band.

Infrared radiation is emitted by all kinds of objects[40]. The IR band has some attributes such as low radiation absorption, higher contrast of the target, and hot target detection, which makes it popular and practical for use in civil and military fields [72]. IR imaging is used in many applications

today, such as object detection, object segmentation, classification, motion detection, etc. However, in contrast to visible band imagery, IR images are not easily accessible because of several reasons. To begin with, the technology of most IR imaging systems is relatively expensive for use in consumer electronics. Besides, since most IR imagery applications are utilized for military or medical applications, they are inaccessible due to either security reasons or intellectual property rights. Hence, the publicly available infrared image and/or video sets are quite limited when compared to high-scale labelled visible band image and video sets.

The main purpose of this article is to compile a list of publicly available infrared image and video sets for artificial intelligence and computer vision researchers. We mainly focus<sup>1</sup> on IR image and video sets which are collected and labelled for computer vision applications such as object detection, object segmentation, classification, and motion detection. We categorize 92 different publicly available or private sets according to their sensor types, image resolution, and scale. We describe each and every set in detail regarding their collection purpose, operation environment, optical system properties, and area of application. To the best of our knowledge, there is no published survey study on infrared image and video sets, their capacity, and their applications. For the reader to completely evaluate different properties of infrared image and video sets, we also provide a background on the fundamentals of infrared imagery including topics such as principles of infrared radiation, infrared sensors, infrared optics, and application fields of IR imagery

The remainder of this paper is organized as follows: Section 2 covers a general overview of IR radiation, IR detectors, IR optics and the related applications. Section 3 starts with analysing the statistical significance of the entire corpus in terms of different categories and follows with providing the image and video sets as a list with brief descriptions for each set. Finally, Section 4 procures a conclusion to the paper.

## 2 Fundamentals of Infrared Imagery

### 2.1 Infrared Radiation

The discovery of IR radiation dates back to an experiment done by Frederick William Herschel more than 200 years ago by using prisms and basic temperature sensors to measure the wavelength distribution of the stellar spectra [19]. However, its widespread use is relatively new starting by the early 20th century with the understanding of Plank's law and blackbody radiation, and also with the help of modern physics and quantum theory [17, 48]. Today it is almost common knowledge that according to certain known laws of physics, objects emit unique radiation in a wide region of wavelengths called the electromagnetic spectrum (ES). The IR region of this spectrum corresponds to wavelengths from the nominal red edge of the visible spectrum around 700 nanometers (frequency 430 THz), to 1 millimetre (300 GHz). IR wavelengths in this region are conventionally categorized into five spectral sub-bands. The wavelength region of  $0.7\mu\text{m}$  to  $1.4\mu\text{m}$  is called the near-infrared (NIR),  $1.4\mu\text{m}$  to  $5\mu\text{m}$ : the short-wave infrared (SWIR),  $3\mu\text{m}$  to  $8\mu\text{m}$ : the mid-wave infrared (MWIR),  $8\mu\text{m}$  to  $15\mu\text{m}$  the long-wave infrared (LWIR), and finally  $15\mu\text{m}$  to  $1000\mu\text{m}$  the far-infrared (FIR) (see Table 1).

The conventional categorization of IR sub-bands defined in Table 1 is correlated with how IR radiation is absorbed, reflected or transmitted by the atmosphere. The region of the IR spectrum, where there is relatively little absorption of terrestrial thermal radiation by atmospheric gases is called the IR atmospheric window, which is roughly between 1 to  $15\mu\text{m}$ . The absorption of IR radiation depends on various atmospheric conditions such as altitude, latitude, solar Zenith angle, water vapor, etc. In Figure 1, a synthetically created spectrum of atmospheric transmission between  $0.7\text{--}30\mu\text{m}$ , using the ATRAN module<sup>2</sup> [59] is depicted. For instance, as seen in Figure 1, atmospheric transmittance of the NIR spectrum band is relatively

<sup>1</sup>Multispectral image sets collected with satellites are left out of the scope of this survey paper. We believe that multispectral satellite imagery is a category that requires a unique focus, due to differences to IR imaging in signal processing practices, perspective, atmospheric effects and applications.

<sup>2</sup>ATRAN module input parameters are selected as, observatory altitude: 13800 feet (Mauna Kea (red) at an altitude of 13.8K feet and 3.4 mm water vapour), observatory latitude: 39 degrees, water vapour overburden: 0 microns, standard atmosphere with 2 Layers, Zenith angle: 45 degrees, smoothing resolution: 1000.

**Table 1:** The IR Spectrum

Wavelength	Designation
$10^{-6}\mu\text{m}$ to $10^{-2}\mu\text{m}$	x rays
$10^{-2}\mu\text{m}$ to $0.4\mu\text{m}$	ultraviolet
$0.4\mu\text{m}$ to $0.7\mu\text{m}$	visible
<b><math>0.7\mu\text{m}</math> to <math>1.4\mu\text{m}</math></b>	<b>NIR</b>
<b><math>1.4\mu\text{m}</math> to <math>3\mu\text{m}</math></b>	<b>SWIR</b>
<b><math>3\mu\text{m}</math> to <math>8\mu\text{m}</math></b>	<b>MWIR</b>
<b><math>8\mu\text{m}</math> to <math>15\mu\text{m}</math></b>	<b>LWIR</b>
<b><math>15\mu\text{m}</math> to <math>1\text{mm}</math></b>	<b>FIR</b>
$1\text{mm}$ to $1\text{m}$	microwaves
$1\text{m}$ to $10\text{km}$	radiowaves

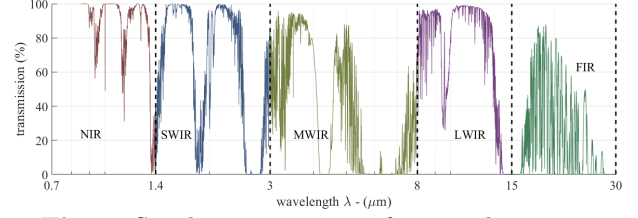
high, which makes this sub-band an effective spectrum for *active* (i.e. an invisible radiation source illuminates the scene) night vision systems.

It is also seen in Figure 1 that much of the IR emission spectrum is unusable because the radiation is absorbed by water or carbon dioxide in the atmosphere. However, there are a number of wavelength bands with low absorption, which actually create the IR sub-bands known as the short, medium and long-wavelength IR bands; abbreviated as SWIR, MWIR and LWIR respectively.

Visible, SWIR or NIR light ( $0.35\text{--}3\mu\text{m}$ ) corresponds to a high atmospheric transmission band and peak solar illumination. This is why most optical systems usually include detectors sensitive to these bands for the best clarity and resolution. However, without moonlight or artificial illumination, SWIR imagers are known to provide poor or no imagery of objects below 300K temperatures. SWIR imaging systems predominantly use reflected light. Accordingly, they are comparable to grey-scale visible images in resolution and detail.

The MWIR (or also referred to as the ‘MIR’) band also offers partial regions with the lossless atmospheric transmission, with the added benefit of lower, ambient, background noise. This region is referred to as the “thermal infrared”. The radiation in this sub-band is emitted from the object itself, hence passive imaging is utilized. Two principal factors determine how bright an object appears in the MWIR spectrum: the object’s temperature and its emissivity (E). Emissivity is a physical property of materials that describes how efficiently it radiates the absorbed radiation.

The LWIR band spans roughly  $8\text{--}15\mu\text{m}$ , with almost no atmospheric absorption between  $9\text{--}12\mu\text{m}$



**Fig. 1:** Synthetic spectrum of atmospheric transmission between  $0.7\text{--}30\mu\text{m}$ , created with ATRAN module [59].

region. Because LWIR sensors can obtain a completely passive image of objects based on thermal emissions only and require no active illumination, this region is also considered as "thermal infrared". LWIR band is better than MWIR for imaging through smoke or atmospheric particles (aerosols). Hence LWIR is usually the chosen technology for surveillance applications. On the other hand, for very long-range detection (such as 10km or more), MWIR has greater atmospheric transmission than LWIR in most atmospheric conditions.

Although the FIR spectrum is defined between  $0.75\mu\text{m}$  and  $1\text{mm}$ , the atmosphere absorbs almost all IR radiation with wavelengths above  $25\mu\text{m}$ . Hence, atmospheric FIR spectroscopy can only be effectively utilized for wavelengths in this limited spectrum. This region is also called a thermal band, which we can experience in the form of heat waves. However, for astronomical observation outside of the atmosphere, the entire FIR spectrum is widely utilized.

For a general overview of the subject and the fundamentals of radiometry, the reader may refer to [70].

## 2.2 Infrared Detectors

One of the fundamental parts of an IR electro-optical system is the detecting sensor. In order to capture the IR signature of a scene, a detector sensitive to IR radiation is needed. IR sensitive detectors capture the IR radiation emitted by the objects and the scene and convert it into electrical signals. Objects that have different temperatures and emissivity, emit different levels of radiation so that the camera produces electrical signals that have different amplitudes. These electrical signals are used to produce the IR image.

**Table 2:** Types of Infrared Detectors

	Type	Properties
Thermal Detectors	Thermocouples, Thermopiles, Bolometers, Pneumatic cells, Pyroelectric Detectors	room temperature operation, low cost, low sensitivity, slow response.
Photon Detectors	Photoconductors, Photodiodes, Schottky Barrier Detectors, Quantum Well IR Photodetectors	low temperature operation, higher cost, higher sensitivity, fast response.

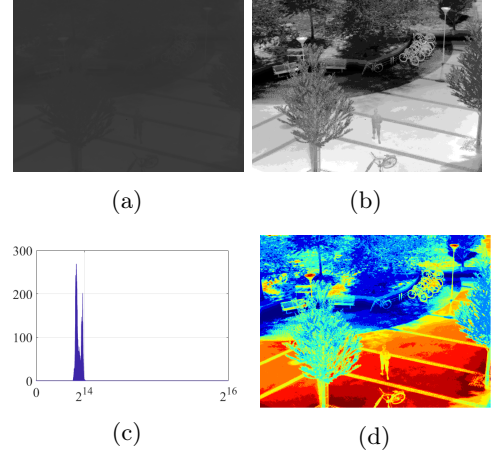
Detectors are the core of an IR imaging system. Historically IR detectors can be scrutinized in three generations. The first generation consists of a single cell detector. In order to create an image plane, the infrared beam emitted from a scene reaches a reflective surface (i.e. mirror). As the position of the mirror is deflected by two-dimensional rotary actuators, the focused infrared beam creates a two-dimensional pattern of the target image plane. In contrast, the second-generation cameras comprise an array of detectors with an optical mirror system that rotates only on a single axis. Finally, the modern third-generation IR optical systems have two-dimensional array detectors, which are known as focal plane arrays (FPA), so that the system does not need a mirror system to scan different parts of the scene [7, 40]. These third-generation optical systems are quite similar to modern digital photographing machines in principle.

In order to measure IR detector performance, three principle metrics are utilized: photosensitivity (or responsivity), noise-equivalent-power (NEP), and Detectivity ( $D^*$ ).

Photosensitivity or responsivity is defined as the output signal per watt of incident energy. The output may vary according to the type of detector, for example, while the output signals in photo-voltaic detectors are usually photocurrent, the output signals in photoconductor detectors are obtained as voltage. Photosensitivity is related to the magnitude of the sensor's response and is expressed as follows;

$$R = \frac{S}{PA} \quad (1)$$

where  $S$  is signal output,  $P$  is incident energy and  $A$  is the detector's active area [40, 94].



**Fig. 2:** (a) A 16-bit raw IR image, (b) its 16-bit raw pixel histogram (x-axis has logarithmic scale), (c) the enhanced image and (d) the false-colour image are depicted. (The picture is taken from The LTIR Dataset [10])

The signal-to-noise ratio (SNR) for a given input flux level is an important parameter used to determine IR image sensitivity [15]. NEP is the quantity of incident light when the SNR is 1 and expressed as follows:

$$NEP = \frac{PA}{S/N \cdot \sqrt{\Delta}} \quad (2)$$

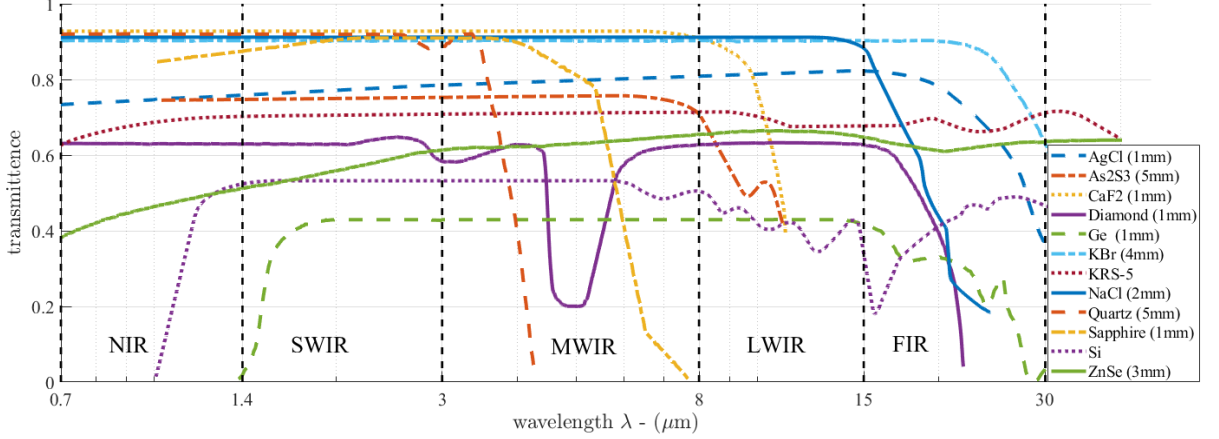
where  $N$  is the noise output and  $\Delta$  is the noise bandwidth (and  $S, P$  and  $A$  are the same as in 1).

Detectivity  $D^*$  (*normalized detectivity*) is the photosensitivity per unit active area of a detector and is expressed as follows:

$$D^* = \frac{\sqrt{A}}{NEP} \quad (3)$$

Technologically, IR detectors are classified into two main groups: thermal detectors and photon (quantum) detectors (see Table 2) [77]. Thermal detectors include thermocouples, thermopiles, pyrometers, bolometers that use infrared energy as heat for detection. They are constructed using metal compounds or semiconductor materials and therefore are low cost. These detectors operate at room temperature. Their sensitivity is independent of wavelengths, therefore, they are capable of capturing scenes in all IR sub-bands. However, they do suffer from slow response times, low sensitivity, and low resolution.





**Fig. 3:** Transmittance of different materials in IR sub-bands.

In contrast to thermal detectors, photon detectors simply count photons of IR radiation. There are different technologies that operationalize these types of sensors such as photoconductors, photodiodes, Schottky Barrier Detectors, and Quantum Well detectors [77]. Compared to thermal sensors, they are more sensitive and operate faster. However, these types of detectors do not operate at room temperature but require a cooling capability. In addition, they are made from materials such as InSb, HgCdTe, and GaAs/AlGaAs whose sensitivity depends on photon absorption and, therefore are more expensive. They also have a limited IR spectrum. Photon detectors are usually utilized when a high sensitivity response is required at a specific wavelength.

Comparative studies on thermal and photon detectors show that both sensor types have their pros and cons [43, 77, 94]. Photon detectors are favoured at specific wavelengths and lower operating temperatures, whereas thermal detectors are favoured at a very long spectral range [76]. Photon detectors are fundamentally limited by generation-recombination noise arising from photon exchange with a radiating background. Thermal detectors are fundamentally limited by temperature fluctuation noise arising from radiant power exchange with a radiating background [52].

### 2.2.1 IR Detector Raw Output

The raw pixel output of an IR detector is the irradiance (i.e. the flux of infrared energy per unit area)

transformed into quantized  $n$ -bit values. These values are within the limits of the so-called “dynamic range”, which is the difference between the largest and smallest signal value the detector can record or reproduce. Hence, the raw pixel values are usually not uniformly distributed within the dynamic range. In practice, a raw IR detector output is usually confined to a very limited range. In Figure 2, a 16-bit IR detector raw output (taken from [10]), its 16-bit raw pixel histogram and the enhanced image are depicted, from left to right.

IR electro-optical systems that provide a visual output for human users, enhance the raw detector output using contrast-enhancing histogram shaping methods [47]. These types of systems usually provide 8-bit contrast-enhanced images as output. However, systems that provide intelligent signal processing algorithms such as tracking, detection, recognition, etc., utilize the raw output of pixels; because the raw output represents the actual irradiance values collected from the scene. The raw output of the electro-optical system usually has the same bit-depth of the IR detector, such as 11-bits or 14-bits. In the following section, when analyzing the various image and video sets, information regarding the raw or enhanced nature of pixel values for a given set is specifically indicated.

Some thermal cameras utilize false colour for their 8-bit contrast-enhanced output. This is usually done for temperature mapping for cameras that are used for temperature measurement. In Figure 2d, an example of a false-colour contrast-enhanced infrared image is depicted.

## 2.3 Infrared Optics

IR imaging technology started in the late 1920s with the understanding of photon emission and improvements continue even today [17]. IR imaging is based on a fundamental concept in geometrical optics called the ray model. A ray model ignores the diffraction and assumes that the lights travel in straight lines from a source point. Each location in the scene can be assumed as a source point, and the source points emit different levels of radiation that create the IR scene.[15].

In geometrical optics an image is constructed via an optical material, by focusing the rays collected from the scene onto an image plane. Hence, the optical material used in an infrared system needs to be transparent (i.e. with transmittance closer to 1.0) at the wavelength the detector is sensitive to. The measure of electromagnetic transmission, a.k.a transmittance, is defined as a percentage of the incident light that passes through a material for a given wavelength of radiation.

When choosing the correct optical material for an IR imaging system, there are three main points to consider. The first is the thermal properties of the material. Usually, optical materials are placed in environments where they are subjected to varying temperatures, hence they may produce a large amount of heat. The materials coefficient of thermal expansion (CTE) should be evaluated to ensure the user is met with the desired performance. Secondly, as mentioned above, sufficient transmittance of the material for the given wavelength is a must. In Figure 3, the transmittance of different materials in IR sub-bands are depicted. For example, if the system is meant to operate in the LWIR band, germanium (Ge) is a better choice than sapphire, which works well in the SWIR band.

Another factor in choosing a suitable optical material is the refractive index, which is the measure of how fast radiation travels through a material. Materials vary in terms of IR refractive index when compared to visible materials, allowing for more variation in system design. That is why, anti-reflection coatings are applied to materials used for IR optics, which also limits them to a small band within the IR spectrum.

For more information on the subject, the reader may refer to [24].

## 2.4 IR Electro-Optical System Properties

There are some important parameters used in selecting appropriate equipment and characterizing the performance of IR systems. The parameters that measure the performance of an IR electro-optical system depend on its ability to detect IR radiation and resolve the temperature differences in the scene. IR images occur due to variations in temperature and emissivity. The parameters that may affect the performance of an IR electro-optical system, in general, include spectral range, normalized detectivity, temperature range, absolute accuracy and repeatability, frame rate, spatial resolution and thermal sensitivity, environment or operating conditions[92]. Below these parameters are briefly explained:

- *Spectral range*: refers to the wavelength range in which the IR system will operate.
- *Normalized detectivity* ( $D^*$ ): as defined in (3), is one of the widely used parameters to compare the performance of IR detectors.
- *Temperature range*: or the *operating temperature*, is the minimum and maximum temperatures that can be measured by the IR system. It has a unit of K,  $^{\circ}\text{C}$ , or  $^{\circ}\text{F}$ .
- *Absolute Accuracy*: is a measure of how accurate the system detects the actual temperature and is denoted by temperature units. Related to this measure, *Repeatability* is defined as the consistency of the system accuracy.
- *Frame rate*: is the number of frames displayed per second. For monitoring moving objects, higher frame rate cameras are mostly preferred[7]. It has a unit of Hz.
- *Spatial resolution*: also referred to as the “instantaneous field-of-view” (IFOV), is the imaging system’s ability to differentiate the details of objects within a single pixel-sized FOV. It is a measure of solid angle, hence represented by steradians. As spatial resolution increases, so does the image quality [7].
- *Thermal sensitivity*: is the smallest temperature change detected by the IR imaging system. There are three most common parameters used as a measure of thermal sensitivity, namely “Noise Equivalent Temperature Difference” (NETD), “Minimum Resolvable Temperature Difference”

**Table 3:** A selection of commercial NIR electro-optical systems and their properties.

Cameras → Parameters ↓	FLIR A35	FLIR T560	FLIR A655SC	FLIR T1010	FLIR A65	FLIR E8-XT
<i>Spectral Range</i>	7.5–13 $\mu\text{m}$	7.5–14 $\mu\text{m}$	7.5–14 $\mu\text{m}$	7.5–14 $\mu\text{m}$	7.5–13 $\mu\text{m}$	7.5–13 $\mu\text{m}$
<i>Detector Type</i>	Uncooled VOx $\mu$ -bol.	Uncooled $\mu$ -bol.	Uncooled $\mu$ -bol.	Uncooled $\mu$ -bol.	Uncooled VOx $\mu$ -bol.	Uncooled $\mu$ -bol.
<i>Field of View (lens size if available)</i>	63°x50°(7.5mm) 48°x39°(9mm) 24°x19.2°(19mm) 13°x10.8°(35mm) 7.6°x6.08°(60mm)	14°x10°	15°x11°	12°x9°	90°x69°(7.5mm) 45°x37°(13mm) 25°x20°(25mm) 12.4°x9.92°(50mm) 6.2°x4.96°(100mm)	45°x34°
<i>Thermal Sensitivity (NETD)</i>	<0.05°C @ 30°C / 50 mK	<50 mK @ 30°C	<30 mK	<25 mK @ 30°C	< 50 mK @ 30°C	<0.05°C / <50 mK
<i>Object Temperature Range</i>	−25↔135°C −40↔550°C	−20↔120°C 0↔650°C 300↔1500°C	−40↔150°C 100↔650°C	−40↔650°C	−25↔135°C −40↔550°C	−20↔550°C (−4↔1022°F)
<i>Measurement Accuracy</i>	± 5°C (± 9°F) or 5 % of reading	±2°C or ±2% of reading	±2°C or ±2 % of reading	± 2 °C or ± 2% of reading	± 5°C (± 9°F) or 5 % of reading	±2°C (±3.6°F) or ±2% of reading
<i>Operating Temperature Range</i>	−15↔60°C	−40↔75°C	−15↔50°C	−15↔50°C	−15↔60°C	−15↔50°C

(MRDT) and “Minimum Detectable Temperature Difference” (MDTD) [92]. It has a unit of temperature (i.e. K, C°, or F°).

In order to choose the right camera for the right application, all of the aforementioned parameters should be taken into account. There are numerous commercial IR electro-optical systems available in the market. In Table 3 we provide a selection of six different near-infrared electro-optical systems, with their comparative parameters, so as to give the reader a sense of the systems engineering perspective of IR electro-optical system selection.

## 2.5 Applications of IR Electro-Optical Systems

As a consequence of the overall development in IR sensing technologies, countless applications have been implemented that can be scrutinized in four main titles, namely, Military & Surveillance, Industrial, Medical, and Scientific. Each title is briefly explained below. The IR image and video sets provided in the next section are categorized according to these application titles.

- *Military & Surveillance Applications:* The military and surveillance field, which also encapsulates law enforcement and rescue applications, cover a vast variety of applications utilized in all IR sub-bands. Warfare applications include

target tracking/detection/acquisition in various platforms such as missiles seeker heads, forward-looking infrared (FLIR) systems, infrared search and track (IRST) systems, directional countermeasure (DIRCM) systems. Regarding law enforcement and rescue applications, night vision systems, reconnaissance and surveillance, fire fighting and rescue in smoke, identification of earthquake victims’ locations, forest fire detection, and radiation thermometer are prime examples.

- *Industrial Applications:* Industrial applications of IR imaging systems include the utilization of IR sensing technology in various industrial fields such as infrared heating in process control, nondestructive inspection of thermal insulators, hidden piping location detection, diseased tree and crop detection, hot spot detection, brake lining, industrial temperature measurement, clear-air turbulence detection, pipeline leak and petrol spill detection, just to name a few.
- *Medical Applications:* The fundamental application of IR technology for medicine is the diagnosis, such as early cancer detection, identification of optimum site for amputation determination, identification of placental site location, early incipient stroke and vein blockage detection,

wound healing monitoring, and infection detection. With the advantage of being non-invasive, IR technology in medicine offers methods that provide useful diagnostic and monitoring information of conditions that are directly or indirectly related to the focused region of the body (such as hands [84]), as well as aiding in the treatment assessment.

- *Scientific Applications*: IR imaging technologies are utilized in almost every scientific field from remote sensing to meteorology, from material science to microbiology, basically from several engineering disciplines to almost every branch of natural science. IR imaging applications that do not include any military, medial or industrial focus belong to this group. Hence, image and video sets that do not have any military surveillance, medical or industrial connection are categorized as scientific in the next section.

### 3 IR Image & Video Sets

In this paper, a total of 92 publicly available or private IR image and/or Video sets are analysed and provided as a list in Table 4. These sets include more than 13 million still images and video frames in total. In this section, before presenting the list with brief descriptions for each set, we provide the statistical details of the compiled list of IR image and video sets in terms of applications fields, including object categories, resolution, annotation and preprocessing details.

Table 4 provides a sample image and a brief description for every set. Some technical specifications such as types of annotated classes, number of total frames, image resolutions(s), Sensor types, image bit depths and application fields for each set are also provided in separate columns. For further information, we recommend the reader refer to the References section for an online link to any of the image sets.

#### 3.1 Application Fields

As mentioned in the previous section, application fields for IR image and video sets are scrutinized in 4 main titles: Military & Surveillance (Mil. & Sur.), Industrial, Medical and Scientific. As seen in figure 4a, the 96.4% of the total volume of the images and video frames fall under the Military and Surveillance category, clearly showing the fact

that a majority of the sets are collected by military and law enforcement units (see Figure 4c). The volume of the sets collected for various scientific applications cover 3.2% of the entire corpus, whereas this share is 0.4% for industrial applications. A marginal share belongs to the medical and industrial applications, which is most possibly related to legal challenges in collecting data for health informatics and industry not choosing to publish their data in public domain<sup>3</sup>. In Table 4, the application fields for every individual set are indicated in the right-most column four (titled “*App.*”).

#### 3.2 Resolution

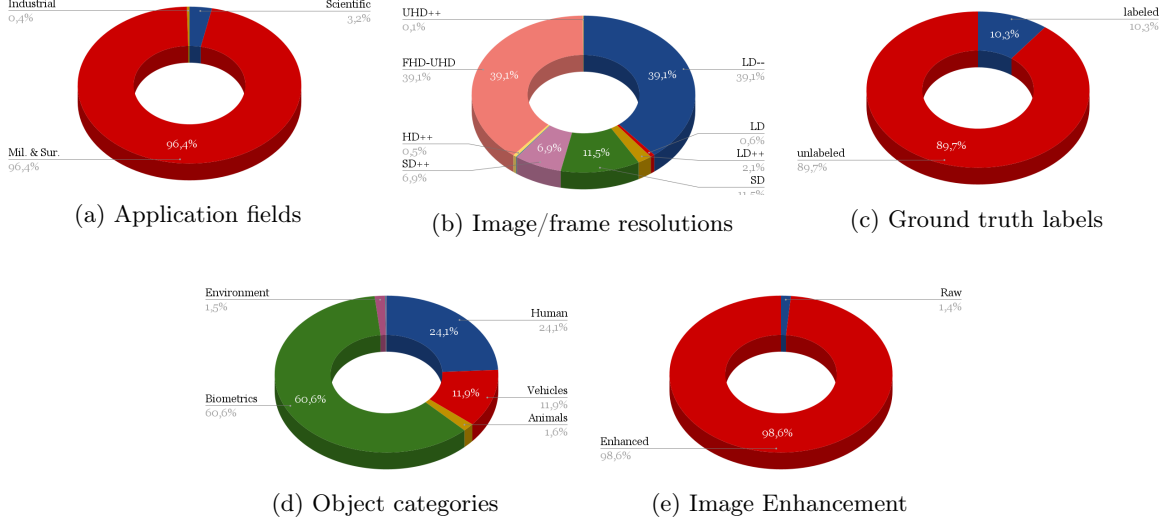
The IR image & video sets listed in this survey vary from low-definition (LD) to Full (HD) or ultra-high-definition (HD) in resolution. Depending on the application, the resolution plays a significant role. Most surveillance systems require HD or better resolutions for accuracy. On the other hand, LD and standard definition (SD) systems are ideal when computational system requirements are limited. Figure 4b shows that the resolutions of the sets are somewhat evenly distributed between HD and LD. We see that almost 40% of the image sets are of LD or lower resolutions, another 40% are HD or higher definition, whereas the rest have resolutions in between (i.e. SD). In Table 4, the actual resolutions for every individual set is indicated in column four (titled “*res*”). In addition, the optical system(s) used to collect the set is provided in column five (titled “*Sensor*”).

#### 3.3 Annotations and Object Categories

In most computer vision applications data are annotated with labels for certain applications such as detection, tracking, recognition etc. Data annotation/labelling is an expensive effort, which provide means for supervised learning, and hence deep learning if the annotated data are sufficiently large in scale. Similarly, some of the IR sets listed in this survey are annotated with various labels. As

---

<sup>3</sup>In Table 4, the “MIntPAIN” [41] including almost 2M frames from 9366 Videos can be considered relevant to both scientific and medical applications. This set is left out of this chart, because it is exceptionally large in volume.



**Fig. 4:** Distributions of various attributes (application field, resolution, ground truth labelling, object category and image enhancement) in the entire collected image/frame corpus are depicted in pie charts.

shown in Figure 4c, about 10% of the entire corpus is annotated. For some sets, these annotations are black-box locations for objects, whereas for some others they are global labels for entire images. Please refer to Table 4 for more individual descriptions (column eight, titled “*Description*”) of the sets.

In Table 4, (in column three, titled “*Classes*”), categories for any existing annotation of a given set is also provided. Annotations of a wide variety of object categories are found in the entire collection of sets. The objects are categorized under 8 titles in Figure 4d, namely biometrics, environments, humans, vehicles, animals, unknown and uncategorized. Biometrics annotations include IR images of faces, irises, ears and/or fingerprints, and cover the majority of the annotations with a 60.6% share. Human annotations, including pedestrians, runners, sportsmen, etc cover 24.1% of these annotations. Vehicles of different sorts such as cars, bicycles, motorcycles, aircraft, boats, etc, are also included and cover 11.9% of label annotations. A small 1.5% share of annotations belong to environmental objects such as terrain, road, clouds etc. A marginal part of the annotations. There are a small number of animal class annotations that take 1.6%. A marginal part (less than 1%) is either some other categories, such as various

objects, food, etc, or uncategorized with labels but include application-specific annotations.

### 3.4 Image Enhancement

As mention previously in Section 2.2.1, IR electro-optical systems that provide a visual output for human users, usually enhance the raw detector output using contrast-enhancing histogram shaping methods. However, systems that provide intelligent signal processing algorithms such as tracking, detection, recognition, etc., utilize the raw output of pixels, which usually has the same bit-depth of the IR detector. Hence raw output is a detector output which is difficult to access in most cases. Unsurprisingly, only 1.4% of the entire volume of collected frames in all listed sets are raw detector outputs. In Table 4, the application fields for every individual set are indicated in the seventh column (titled “*bit*”) provides information about the bit depth of the images/frames of a given set. The number (8, 16, etc.) corresponds to image bit-depth. The abbreviation “HE” is to indicate histogram enhancement processes, whereas the phrase “RAW” indicates the existence of the raw detector output. For some sets, the bit depth is indicated by “8\*” showing that the images/frames are of 24bit RGB (i.e 8bit per channel) format.



**Table 4:** Available IR image and video sets for different application fields. From left to right, the columns depict the name and the reference, a sample image, the included object classes (if any), total number of frames, pixel resolution of images, the optical system (if specified), pixel bit depth (and if any histogram equalization - HE applied), a brief description and the application fields of the given dataset, respectively.



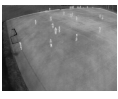

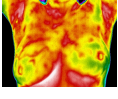

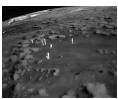


Name	Sample	Classes	# fr.	res.	Sensor	bit	Description	App.
AAIart Data [103]		pedestrian	771	640x513	Catherine MP LWIR	8 HE	The dataset includes thermal infrared video sequences comprising of pedestrians and various types of vehicles for an infrared surveillance system that can be widely applied in military applications.	Mil. & Sur.
AAU RainSnow [8]		vehicle	4.5K	640x480	not specified	8* HE	The image set includes traffic surveillance images (RGB+thermal) and 22 video pairs in rainfall and snowfall from seven different traffic intersections at the Danish cities of Aalborg and Viborg. The purpose of the dataset is detection and classification under challenging weather conditions. The dataset includes pixel-level annotations. Totally, 2,200 frames, containing 13,297 objects, are annotated.	Mil. & Sur.
AAU-PD-T [42]		vehicle, pedestrian	3K	384x288 640x480	Axis Q1921 Axis 1922	8* HE	The image set contains approximately 3k thermal pedestrian images with a total of 5590 person annotations. Training data is divided into 9 categories, such as good weather, far viewpoint, occlusions, snow, wind, just to name a few.	Mil. & Sur.
ASL-TIR [73]		human, cat, horse	4381	324x256	FLIR Tau 320	8/16 HE/RAW	ASL thermal IR dataset includes 8 sequences of thermal images of humans, cats and horses, with manually annotations. The images are captured at indoor and outdoor environments.	Mil. & Sur.
BCT [35]		breast	60	640x480	Infrec R500	8 HE	The dataset contains thermal breast images of 60 patients for breast cancer detection.	Medical
BERTIN [23]		vehicle, pedestrian	more than 10K	320x240	FLIR A20M	16 RAW	The dataset includes both visible and thermal images of pedestrians and vehicles, captured with a static and a moving camera. Contains training, validation and test sets with their ground truths. For access, Robin Competition participation is required.	Mil. & Sur.
BIRDSAI [14]		human, animal	160K	640x480	FLIR Vue Pro 640 Tamarisk 640	8 HE	The dataset consists of two parts, real and synthetically created, with annotations. The real data includes 48 thermal infrared videos sequences of humans and animals, captured with a thermal camera mounted on a UVA, that flies over African landscapes. The synthetic data, generated with MS AirSim simulation platform, include 124 thermal infrared video sequences.	Scientific
BU-TIV [98]		motorcycle, runner, car, bicycle, pedestrian	35K 2999 6000 1275 1282	up to 1024x1024	FLIR SC8000	16 RAW	The dataset contains various tasks, such as single object detection, multi-object detection, motion detection, counting, that describes real world scenarios such as a marathon runner, people walking down a hall, etc., with ground truth data. In addition, the set includes images of bats for tracking and counting throughout the sequence.	Mil. & Sur.
		bat	19K					Scientific




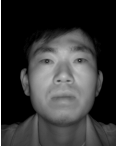


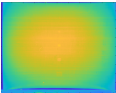



Table 4	continued...							
CAMEL [34]		biker, vehicle, pedestrian	44.5k	336x256	FLIR Vue Pro	8* HE	The dataset contains 26 videos sequences, captured in an urban environment, in the visible and thermal infrared domains, with their annotations.	Mil. & Sur.
Carl Database [30]		face	7380	640x480	TESTO 880-3	8* HE	Contains visible and thermal images of human faces, with constant 135 cm distance from the sensor, in front of a matt black background.	Mil. & Sur.
CATS [96]		vehicles, pedestrians, other	1520	640x480	Xenics Gobi 640 GigEs	16 RAW	The dataset contains stereo thermal, stereo color, and cross-modality images of pedestrians, vehicles, and some other objects in different weather conditions.	Mil. & Sur.
CBSR NIR [55]		face	4K	480x640	not specified	8 HE	The dataset contains NIR images from 197 people, collected for face detection, eye detection and face recognition tasks.	Mil. & Sur.
CDW 2014 [95]		pedestrian	21K	320x240 → 720x576	not specified	8* HE	The 2014 CDnet dataset, which is extended version of CDnet 2012 dataset, contains 11 video categories, one of which is the Thermal category, that contains 5 video sequences (3 outdoor + 2 indoor) shot by a far infrared camera annotated with pedestrian bounding boxes.	Mil. & Sur.
Cheetah [75]		cheetah	129	416x416	Seek Compact XR	8 HE	This dataset is a collection of thermal infrared images and video frames of cheetahs.	Mil. & Sur.
Comp-Mat [28]		composite materials	2000	512X512	FLIR X6900	8 HE	The dataset consists of 12 image sequences collected for locating laminar defective regions from composite materials. The IR camera records the thermal evolution of both sides of the sample for a few seconds for 3 stages, before a heat pulse, during the heat pulse and after the heat pulse.	Industrial
CSIR CSIO [3]		vehicle, human, dog, bird	3650	640x480	Uncool. p-bol	8* HE	A moving object detection dataset which has 18 sequences of moving targets, four, three and two-wheelers, pedestrians and some animals. Thermal infrared videos were captured at the coastal area of the Bay of Bengal in Southern India with a sample rate of 10hz.	Mil. & Sur.
CVC-09 [83]		pedestrian	10K	640x480	not specified	8 HE	FIR Sequence Pedestrian Dataset include two sequences, day and night, captured at urban areas. Each sequence has about five thousand frames, divided into distinct train and test sets.	Mil. & Sur.
CVC-14 [38]		pedestrian	8400	471x640	not specified	8 HE	Visible-FIR Day-Night Pedestrian Sequence dataset includes two sequences of 3695 day images and 3390 night images, with pedestrians annotated, again divided into distinct train and test sets.	Mil. & Sur.




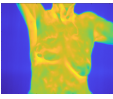
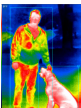

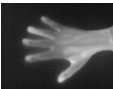

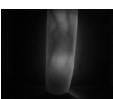


Table 4	continued...							
DDPM [85]		face	8M	80x60 1920×1080	DMK 33UX290 FLIR C2	8 HE	The dataset includes RGB and IR face videos of 13 hours of recordings of 70 subjects an interview scenario in which the interviewee attempts to deceive the interviewer on selected responses. Besides the RGB and IR videos, the set includes various biometric sensor records. Registration required.	Mil. & Sur.
DIAST [5]		ear	2200	125x125	FLIR E60	8 HE	The DIAST dataset contains visible and thermal ear images taken from a side face profile, from 55 subjects, collected for the task of ear recognition.	Mil. & Sur.
Dim Small Air. [44]		aircraft	16K	256×256	not specified	8* HE	The dataset includes 22 sequences with sky and open-field backgrounds for infrared aircraft detection and recognition tasks.	Mil. & Sur.
DMR-IR [93]		breast	1522	640x480	FLIR SC-620	8 HE	The dataset consists of thermal breast images to be used for breast cancer diagnosis.	Medical
Dogs [66]		pedestrian, dog	203	416x416	Seek Compact XR	8 HE	The dataset includes thermal infrared person and dog images captured in outdoor environments.	Mil. & Sur.
EADS [23]		plane, vehicle	not specified	not specified	not specified	8 HE	The dataset contains aerial images of vehicles, planes etc, for object detection tasks. Training and validation sets are provided with ground truths. Registration required.	Mil. & Sur.
Focus-Obj [29]		circuits, heater, face, hand, etc.	960	160×120	TESTO 880-3	8 HE	The database consists of several image sets. In each set, the camera acquires one image of the scene at 96 different lens positions.	Industrial
FREE FLIR [31]		vehicle bicycle dog pedestrian	14K images 10k short videos	up to 1280x1024	IR Tau2 FLIR BlackFly	8/14 HE/RAW	The dataset contains 8 bit RGB and 8/14 bit thermal images images, with annotations. The images are captured on streets and highways of Santa Barbara, CA area, in different weather conditions, during day and night.	Mil.& Sur. Industrial
FV-USM [63]		Finger Vein	5904	640x480	not specified	8* HE	The dataset contains infrared finger images of 83 male and 40 female volunteers for finger vein recognition tasks.	Mil. & Sur.
HGRD [60]		hand	20K	640×240	not specified	8 HE	The Hand Gesture Recognition Dataset (HGRD) includes near infrared images of 10 different gestures, performed by 10 different subjects (5 men and 5 women). It has 200 frames for each subject and of each hand gesture.	Industrial
HS-NIR [39]		coffee bean, sugar, floor, salt	480	192x256	AHS- U20MIR	8 HE	The dataset provides a total of 480 images of 5 objects. For each object there are 96 different NIR hyperspectral images.	Industrial


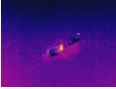
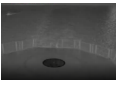


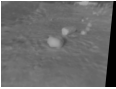


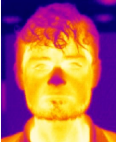

Table 4	continued...							
IIT Delhi [53]		face	612	768x576	not specified	8 HE	The database contains face images, captured in IIT Delhi campus with a webcam, shot with NIR-only illumination.	Mil. & Sur.
Illegal Fishers [4]		fishing gear, ship	84	640x480 4056x3040	not specified	8* HE	The dataset has raw thermal, visible, and night vision images captured by a drone with a thermal camera to detect the illegal fishing in Kuwaiti Bay.	Mil. & Sur.
IPATCH [71]		boat	not specified	640x480 640x512	FLIR SC655 FLIR A65	not specified	The IPATCH dataset contains 14 thermal videos from the coast of Brest, France, for object detection and tracking, event detection, and threat recognition tasks of maritime piracy. There are selected sequences of abnormal events, such as boat speeding up, boat loitering, boat moving around vessel, etc.	Mil. & Sur.
IRIS [49]		face	4228	320x240	Raytheon Palm IR Pro	8* HE	The dataset consist of thermal and visible face images with various expressions, poses and illumination conditions.	Mil. & Sur.
IRShips [97]		ship	972K	1024x512	N/A	8 HE	This dataset contains synthetically generated IR images of 10 different ships.	Mil. & Sur.
JPL [46]		sand, soil, rocks, bedrock, rocky terrain, etc.	1300	800x600	FLIR AX65	8 HE	The dataset comprises of IR and RGB images, in 2 parts: 1) the Semantic Dataset for Terrain Types and 2) the Virtual Sensor Dataset for deriving RGB-to-IR mapping models. Semantic Dataset includes manually annotated 7 categories, such as unlabeled, sand, soil, rocks, bedrock, rocky terrain, and ballast.	Scientific
KAIST [45]		pedestrian	95K	320x256	FLIR A35	8 HE	The dataset contains multispectral images of vehicles captured in day and night traffic with annotations.	Mil. & Sur.
Kayak Image Fusion [89]		kayak	2541	up to 752x582	Raytheon Rad. HS AEG AIM 256 PLW Philips LTC500	8-8* HE	The dataset includes two sequences with several kayaks in a maritime. The images are captured in MWIR, LWIR and visible domains.	Mil. & Sur.
L-CAS FACE [22]		face	3000	382x288	Optris PI-450	8 HE	The dataset comprises of thermal images of moving faces, captured with a sensor that is mounted on the top of a robot to measure respiration and heart-beat rate for physiological monitoring. The dataset provides ground truth for respiration and heartbeat.	Mil. & Sur.
L-CAS ReID [21]		person	36K	382x288	Optris PI-450	8 HE	The dataset includes RGB, depth, and thermal images of people for re-identification tasks. The set is collected via a thermal camera on a robot.	Mil. & Sur.

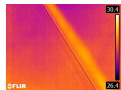



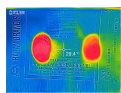

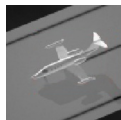

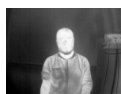



Table 4	continued...							
Leaves [2]		leaf	636	320x240	FLIR E8	8 HE	The dataset, composed of thermal leaf images, categorized by 6 categories, bacteria leaf blight, blast, leaf spot, leaf folder, hispa, healthy leaves.	Industrial
LSI [67]		pedestrian	20K	32x64 164x128	not specified	16 RAW	The set consists of FIR pedestrian images in an outdoor urban environment, divided into train and test sets, with manually annotated bounding boxes.	Mil. & Sur.
LSOTB TIR [58]		person, animal, vehicle, aircraft, boat	600K	not specified	not specified	8 HE	The dataset consists of various objects classes, with 730K bounding box annotations in total, shot in different environments, such as urban areas, forests, the sea, etc.	Mil. & Sur.
LTIR [10]		rhino, human, horse, car, quadcopter, dog	11K	up to 1920x480	FLIR A35 FLIR Tau320 FLIR A655SC	8/16 HE/RAW	The dataset includes 20 thermal IR sequences of different objects, captured at indoor and outdoor environments, with manual benchmark annotations.	Mil. & Sur.
Mango [64]		mango	309	640x480	FLIR One	8* HE	The dataset consists of thermal mango images for object counting and color feature extraction.	Industrial
MBD [78]		fingerprint, finger-vein, face, iris	72	up to 640x480	not specified	8/8*/32 HE	The set includes 45 thermal finger prints, 9 thermal finger veins, 9 thermal iris, and 9 thermal face images.	Mil. & Sur.
MBDA [23]		plane, helicopter, vehicle, tower	>15K	320x240 256x256	N/A	14/16 RAW	The dataset contains computer-generated aircraft and vehicle images. Train and validation sets are provided with ground truths. Registration required.	Mil. & Sur.
METU [101]		various objects	24	640x480	Kinect	8 HE	METU Kinect dataset consists of IR and visible image pairs of several objects.	Scientific
MIntPAIN [41]		person, face	2M (9366 vid.)	640x480	Axis Q 1922	8 HE	The MIntPAIN is an RGB, Depth and Thermal (RGBDT) image set, which contains RGBDT videos of 20 subjects. Each subject has 80 folders in visible, depth, and thermal domains for pain level recognition tasks. Registration required.	Med.& Sci.
MM-Bio [20]		face	2500	not specified	FLIR E40	8 HE	Multi-model biometrics dataset contains thermal and RGB face images of 125 people. Registration required.	Mil. & Sur.
MM-Hand [1]		hand	65K	412x273	not specified	8 HE	Multi-modal Hand Gesture Recognition dataset presents near-infrared images of 15 different hand gestures from 15 different subjects (5 women and 10 men).	Scientific
Mov-Tar [88]		vegetation, building	150K	640x512	not specified	8 HE	The dataset includes IR background images, in which synthetic small infrared targets are embedded for target detection and tracking applications.	Mil. & Sur.





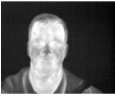








Table 4	continued...							
MS Focus [106]		building, car, corri- dor, head, keyboard, office desk, pens	420	640x480	Canon EOS 350D FLIR SC660	8 HE	This database contains 420 images of 7 objects in different focus positions, captured in visible, near-infrared, and thermal spectrum.	Industrial
Multi-Focus [9]		uncate- gorized	576	320x240	TESTO 882-3	8 HE	The set consists of six image sets acquired at different lens positions, by manually moving the lens in 1 mm steps. Each set consists of 96 different images of the one scene.	Industrial
ND X1 [18]		face	4584	not specified	Merlin uncooled $\mu$ -bol.	8 HE	The set includes 2292 IR and 2292 visible face images from 82 subjects.	Mil. & Sur.
ND-NIVL [11]		face	25K	4770x3177 4288x2848	Nikon D90 Canon EOS 50D	8 HE	The dataset includes RGB face images obtained from 574 subjects and NIR face images obtained from 230 subjects. There are 2341 frames in the visible domain and 22264 frames in the IR domain.	Mil. & Sur.
NTU RGB+D [80]		120 human actions	114K	512x424	Kinect V2	8 HE	The dataset contains RGB videos, depth map sequences, 3D skeletal data, and infrared (IR) videos of 82 daily actions, 12 medical conditions, and 26 mutual actions. To access this dataset, you must get a LoginID.	Scientific
OSU-CTD [26]		vehicle, pedestrian	17089	320x240	Raytheon PalmIR 250D	8* HE	OSU Color-Thermal Database (CTD) dataset includes 6 color/thermal sequences, captured 3 at each location, utilized for fusion and fusion-based object detection in color and thermal imagery.	Mil. & Sur.
OSU TPD [25]		pedestrian	284	360x240	Raytheon 300D	8 HE	OSU Thermal Pedestrian Database (TPD) dataset includes 10 sequences of IR pedestrian videos with ground truth data, for only those people who were at least %50 visible in the image.	Mil. & Sur.
OTCBVS-P [13]		pedestrian	5390	480x360	FLIR A40M	8* HE	Pedestrian Infrared/visible Stereo Video dataset contains 4 visible and infrared video sequences of several people walking with 206 annotated frames and 25819 ground-truth point pairs.	Mil. & Sur.
Parma [12]		pedestrian	18K	320x240	not specified	not specified	Parma Tetravision dataset, includes visible and infrared images captured from a car, with pedestrian annotations.	Mil. & Sur.
PETS 2005 [86]		vehicle	5K	320x256	not specified	8* HE	This an aerial vehicle tracking dataset containing 6 visible and 3 thermal infrared video sequences with ground-truth.	Mil. & Sur.
PTB-TIR [57]		vehicle, pedestrian	30128	up to 1280x720	8 dif. cams.	8 HE	TIR pedestrian tracking dataset include manually annotated 60 thermal sequences, divided into nine subsets with different shooting properties. The images are captured indoor and outdoor environments with surveillance, hand-held, vehicle-mounted and drone cameras during day and night.	Mil. & Sur.



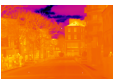








Table 4	continued...							
RGB-NIR [16]		building, mountain, tree, car, motorcycle, etc.	477	1024x768	Canon T1i	8* HE	The dataset contains RGB and NIR images of 9 categories: country, field, forest, indoor, mountain, old buildings, street, urban, water. Some frames include objects like buildings, trees, cars and motorcycles.	Scientific
RGBT Salient [91]		various objects	5000	640x480	FLIR T640 T610	8 HE	This dataset contains 5000 thermal/RGB image pairs with ground truth annotations of various objects like sneakers, pontoon, stool, dustbin, headphones for salient object detection tasks.	Scientific
RIFIR [62]		pedestrian	20K	640X480	not specified	8* HE	The dataset contains sequences of images, captured in an urban environment with one Far Infrared and two color cameras. There are train and test sets, with annotated pedestrian in the Visible and IR domain.	Mil. & Sur.
SAGEM [23]		vehicle, etc.	1400	384x256	MWIR Matis	16 RAW	The dataset contains 16bits IR aerial images of vehicles for classification and detection tasks.	Mil. & Sur.
SCUT-FIR [100]		pedestrian	211K	720x576	NV628	8 HE	The dataset consists of approximately 11-hour long image sequences captured in various traffic scenarios. Images were captured 11 road sections in various environments including the city center, suburbs, highway, and campus.	Mil. & Sur.
SDT [87]		person	48K	640x480	FLIR Lepton 3.5	16 RAW	The dataset includes 40k synthetic and 8k real depth and thermal stereo images for human behavior recognition and person detection tasks, bedroom, bathroom, and kitchen. It provides person bounding box annotations.	Mil. & Sur.
SENSIAC [79]		people, vehicles, etc	not publicly specified	not publicly specified	not publicly specified	not publicly specified	The dataset contains 207 GB of videos in the IR domain and 106 GB of videos in the visible domain with ground truth data for automatic target recognition (ATR) tasks. It was collected by the US Army Night Vision and Electronic Sensors Directorate (NVESD). No public access	Mil. & Sur.
Server [56]		server hardware	1351	320x240	FLIR E8	8* HE	The dataset contains thermal images of servers for detecting the overheated area of the server surface, with five categories: normal status, main fan failure, vice-fan failure, air vent blockage and low-load status.	Industrial
SG-Ship [74]		ship	24300	1080x1920	Canon 70D	8* HE	Singapore Maritime dataset The ships videos, captured at various locations around Singapore waters. The set is divided into three parts, 40 videos for visible on-shore, 11 videos for visible on-board and 30 videos for NIR on-shore shots. The dataset provides annotations in .mat format in 3 folders: horizon, object and track.	Mil. & Sur.
Soccer [32]		people	3000	1920x480	AXIS Q1922	8 HE	The dataset provides four thermal infrared video sequences of eight soccer players at an indoor sports arena.	Mil. & Sur.
Spindle [99]		lathe milling	1500	640x480	not specified	8* HE	Spindle thermal error prediction dataset contains all the thermal images and error data of a spindle, taken on a lathe and a milling machine.	Industrial

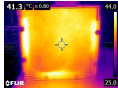



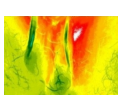
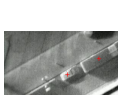

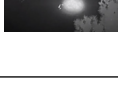
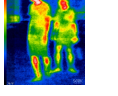

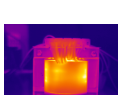








Table 4	continued...							
Surf-Coat [82]		various materials	449	320x240	FLIR E4	8* HE	This dataset contains raw temperature measurement data of external, internal surfaces and air in the interior of a structure under different conditions. It has also surface thermographic images of different types of coatings and diffuses reflectance data for these materials. It has amplified images of the surfaces.	Industrial
Terravic-F [61]		face	23K	320x240	Raytheon L3	8 HE	The Terravic Facial dataset consist of 20 thermal infrared facial image sequences, captured from the front, left and right at indoor and outdoor environments.	Mil. & Sur.
Terravic-M [61]		human, plane, dock	22K	320x240	Raytheon L3	8 HE	The Terravic Motion dataset has 18 sequences of thermal infrared images, captured at indoor and outdoor environments for object detection and tracking tasks.	Mil. & Sur.
Terravic-W [61]		person, weapon	3555	320x240	Raytheon L3	8 HE	The dataset includes 5 thermal IR image sequences for weapon detection and weapon evacuation detection tasks.	Mil. & Sur.
TestisT [36]		testis	50	640x320	VIS-IR 640	8 HE	The Testis Thermography dataset contains 50 thermal testis images to detect varicocele.	Medical
THALES [23]		vehicle, boat	more than 6K	320x240 320x256 640x512	not specified	8/16 HE/RAW	The dataset consists of comprise aerial images, obtained from a six hours video recorded from helicopter at different environments, such as urban, expressway, rural etc. Registration required.	Mil. & Sur.
The Flame [81]		fire	49K	640x512 3840x2160	FLIR Vue Pro R DJI Phantom 3	8* HE	The dataset consists of raw aerial video and raw heat map footage captured by drones, during a pile burn in Northern Arizona, to detect wildfires. It has 47992 labeled frames for fire classification and 2003 ground truth mask frames for fire segmentation.	Mil. & Sur.
TIDOC [6]		car, cat, pedestrian	6892	300x400 1080x1440	FLIR Seek Thermal	8* HE	The Thermal Image dataset for Object Classification (TIDOC) includes thermal images of three classes, car, cat, and man.	Mil. & Sur.
TIRDRD [102]		road	6000	640x480	FLIR A655SC	8 HE	Thermal IR-based Drivable Region Detection dataset consists of about 6000 manually annotated images, with road scenarios, such as on-road, off-road, and cluttered road for the drivable region detection task.	Mil. & Sur.
Transformer [65]		transformer, induction motors	255	320x240	Dali-tech T4/T8	8* HE	The dataset contains thermal images of induction motors and transformers for the purpose of condition monitoring.	Industrial
TRICLOBS [90]		people, vehicle	57K	640x480	XenICs Gobi 384	8 HE	The TRICLOBS (TRI-band Color Low Light OBServation) dataset contains video sequences in visible, NIR and LWIR bands. The main purpose of this dataset is to use image fusion and color mapping algorithms for surveillance applications.	Mil. & Sur.

Table 4	continued...							
Tufts-Face [69]		face	100K	not specified	various cameras	not specified	Tufts-Face-Database has more than 100K face images of 7 image modes: visible, NIR, thermal, computerized sketch, video, plenoptic and 3D images.	Mil. & Sur.
UL-FMTV [37]		face	71400	640x512	Indigo Phoenix Thermal	8 HE	The ULFMT video dataset includes MWIR band facial videos of 238 subjects for facial pose and expression recognition applications.	Mil. & Sur.
UNIRI-TID [51]		person	11K	1280x960	FLIR Therma -Cam P10	8 HE	This is a set of thermal videos and images that simulate illegal movements around the border and in protected areas. The videos are recorded in areas around the forest, at night, in different weather conditions.	Mil. & Sur.
VAIS [105]		ship	1242	1024x680	Sofradir EC Atom 1024	8 HE	VAIS contains IR and visible images sequences of real-world ship images captured from piers, with annotations.	Mil. & Sur.
Valle-Aerial [33]		road, car	110	336x256	Zenmuse XT	8* HE	The dataset is composed of thermal and visible aerial images, with their metadata, captured using the UAV of a planar scene at Universidad del Valle, Cali, Colombia.	Mil. & Sur.
VAP [68]		people	11537	640x480	AXIS Q1922	16/32 HE/RAW	The dataset contains RGB (32bit), depth (16bit), and thermal (32bit) images of people for human detection, human segmentation, person re-identification tasks, with 5724 annotated frames.	Mil. & Sur.
VivID++ [54]		uncate- gorized	9290	640x480	FLIR A65	8 HE	The dataset provides normal and poor illumination sequences, captured by thermal, depth, and temporal difference sensors for indoor and outdoor environments.	Scientific
VOT-RGBTIR [50]		pedestrian, bike, car, dog, motorcycle	20K	around 600x400	not specified	8* HE	VOT-RGB TIR 2019 dataset includes infrared images in 60 sequences. Each sequence contains various numbers of images with objects like cars, pedestrians, motorcycles, etc. The dataset has different object annotations, such as baby, child or cars with colour, etc.	Mil. & Sur.

## 4 Conclusion

In this survey, we compile a list of publicly available IR image and video sets for artificial intelligence and computer vision researchers. We mainly focus on IR image and video sets, which are collected and labelled for computer vision applications such as object detection, object segmentation, classification, and motion detection. We categorize 92 different publicly available or private sets according to their sensor types, image resolution, and scale. The list includes brief descriptions for each

set, the statistical details of the entire corpus of IR image & video sets are provided in terms of applications fields, including object categories, resolution, annotations, sensor types and preprocessing details.

We believe that this survey, with solid introductory references to the fundamentals of IR imagery, will be a guideline for computer vision and artificial intelligence researchers that would want to delve into working with the spectra beyond the visible domain. As a future direction, this collection can be used to study deep learning models that

would require very large-scale sets, for problems such as IR domain adaptation, multi-modal vision and fusion.

## References

- [1] (2018) Multi-modal dataset for hand gesture recognition. Available at <https://www.kaggle.com/gti-upm/multimodhandgestrec>
- [2] (2020) Thermal images - diseased & healthy leaves - paddy. Available at <https://www.kaggle.com/sujaradha/thermal-images-diseased-healthy-leaves-paddy?select=thermal+images+UL>
- [3] Akula A, Khanna N, Ghosh R, et al (2014) Adaptive contour-based statistical background subtraction method for moving target detection in infrared video sequences. *Infrared Physics & Technology* 63:103–109. Available at <http://vcipl-okstate.org/pbvs/bench/>
- [4] Alqattan M (2020) A dataset of raw thermal, visible and night vision images for illegal fishers in the kuwaiti bay. <https://doi.org/10.17632/69ncy4nxsg.1>, Available at <https://data.mendeley.com/datasets/69ncy4nxsg/1>
- [5] Ariffin SMZSZ, Jamil N, Rahman PNMA (2016) Diast variability illuminated thermal and visible ear images datasets. In: 2016 Signal Processing: Algorithms, Architectures, Arrangements, and Applications (SPA), pp 191–195, <https://doi.org/10.1109/SPA.2016.7763611>, Available at <http://vcipl-okstate.org/pbvs/bench/>
- [6] Ashfaq Q, Akram U, Zafar R (2021) Thermal image dataset for object classification. <https://doi.org/10.17632/btmrycjbj.1>, Available at <https://data.mendeley.com/datasets/btmrycjbj/1>
- [7] Bagavathiappan S, Lahiri B, Saravanan T, et al (2013) Infrared thermography for condition monitoring—a review. *Infrared Physics & Technology* 60:35–55
- [8] Bahnsen CH, Moeslund TB (2018) Rain removal in traffic surveillance: Does it matter? *IEEE Transactions on Intelligent Transportation Systems* pp 1–18. <https://doi.org/10.1109/TITS.2018.2872502>, Available at <https://www.kaggle.com/aalborguniversity/aau-rainsnow/>
- [9] Benes R, Dvorak P, Faundez-Zanuy M, et al (2013) Multi-focus thermal image fusion. *Pattern Recognition Letters* 34(5):536–544. Available at <http://splab.cz/en/download/database/multi-focus-thermal-image-database>
- [10] Berg A, Ahlberg J, Felsberg M (2015) A thermal object tracking benchmark. In: Advanced Video and Signal Based Surveillance (AVSS), 2015 12th IEEE International Conference on, Available at <http://www.cvl.isy.liu.se/en/research/datasets/ltir/version1.0/>
- [11] Bernhard J, Barr J, Bowyer KW, et al (2015) Near-ir to visible light face matching: Effectiveness of pre-processing options for commercial matchers. In: 2015 IEEE 7th International Conference on Biometrics Theory, Applications and Systems (BTAS), pp 1–8, <https://doi.org/10.1109/BTAS.2015.7358780>, Available at <https://cvrl.nd.edu/projects/data/>
- [12] Bertozzi M, Broggi MVGDRMA.and Felisa (2006) Low-level pedestrian detection by means of visible and far infra-red tetra-vision. Maintained by <http://vislab.it/>
- [13] Bilodeau GA, Torabi A, St-Charles PL, et al (2014) Thermal–visible registration of human silhouettes: A similarity measure performance evaluation. *Infrared Physics & Technology* 64:79–86. Available at <http://vcipl-okstate.org/pbvs/bench/>
- [14] Bondi E, Jain R, Aggrawal P, et al (2020) Birdsai: A dataset for detection and tracking in aerial thermal infrared videos. In: WACV, Available at <https://sites.google.com/view/elizabethbondi/dataset>



- [15] Boreman GD (1998) Basic electro-optics for electrical engineers, vol 31. SPIE Press
- [16] Brown M, Süssstrunk S (2011) Multispectral SIFT for scene category recognition. In: Computer Vision and Pattern Recognition (CVPR11), Colorado Springs, pp 177–184, Available at [https://ivrlwww.epfl.ch/supplementary\\_material/cvpr11/index.html](https://ivrlwww.epfl.ch/supplementary_material/cvpr11/index.html)
- [17] Buser RG, Tompsett MF (1997) Historical overview. In: Semiconductors and Semimetals, vol 47. Elsevier, p 1–16
- [18] Chen X, Flynn P, Bowyer K (2005) Ir and visible light face recognition. Computer Vision and Image Understanding 99:332–358. <https://doi.org/10.1016/j.cviu.2005.03.001>, Available at <https://cvrl.nd.edu/projects/data/>
- [19] Clerke AM (2003) A popular history of astronomy during the nineteenth century. Sattre Pr
- [20] Computer Vision and Biometrics Lab. (2022) Multimodal biometrics dataset thermal face images. Available at <https://cvbl.iitit.ac.in/dataset.php>
- [21] Cosar S, Bellotto N (2019) Human re-identification with a robot thermal camera using entropy-based sampling. Journal of Intelligent & Robotic Systems <https://doi.org/https://doi.org/10.1007/s10846-019-01026-w>, Available at <https://lcas.lincoln.ac.uk/wp/research/data-sets-software/l-cas-rgb-d-t-re-identification-dataset/>
- [22] Coşar S, Yan Z, Zhao F, et al (2018) Thermal camera based physiological monitoring with an assistive robot. In: 2018 40th Annual International Conference of the IEEE Engineering in Medicine and Biology Society (EMBC), pp 5010–5013, <https://doi.org/10.1109/EMBC.2018.8513201>, Available at <https://lcas.lincoln.ac.uk/wp/research/data-sets-software/>
- [23] D’Angelo E, Herbin S, Ratieville M (2006) Robin challenge. Available at <https://robin.inrialpes.fr/testsdefinitions.php>
- [24] Daniels A (2018) Field Guide to Infrared Optics, Materials, and Radiometry, vol FG39. SPIE
- [25] Davis JW, Keck MA (2005) A two-stage template approach to person detection in thermal imagery. In: 2005 Seventh IEEE Workshops on Applications of Computer Vision (WACV/MOTION’05)-Volume 1, IEEE, pp 364–369, Available at <http://vcip-okstate.org/pbvs/bench/>
- [26] Davis JW, Sharma V (2007) Background-subtraction using contour-based fusion of thermal and visible imagery. Computer vision and image understanding 106(2-3):162–182. Available at <http://vcip-okstate.org/pbvs/bench/>
- [27] Dodge SF, Karam LJ (2017) A study and comparison of human and deep learning recognition performance under visual distortions. CoRR abs/1705.02498. URL <http://arxiv.org/abs/1705.02498>, <https://arxiv.org/abs/1705.02498>
- [28] Erazo-Aux J, Loaiza-Correa H, Restrepo-Giron AD, et al (2020) Thermal imaging dataset from composite material academic samples inspected by pulsed thermography. Data in brief 32:106,313. <https://doi.org/10.1016/j.dib.2020.106313>, URL <https://europepmc.org/articles/PMC7508994>, Available at <https://data.mendeley.com/datasets/v4knrwgj9y/2>
- [29] Faundez-Zanuy M, Mekyska J, Espinosa-Duró V (2011) On the focusing of thermal images. Pattern Recognition Letters 32:1548–1557. <https://doi.org/10.1016/j.patrec.2011.04.022>, Available at <http://splab.cz/en/download/database/thermal-focus-image-database>
- [30] Faundez-Zanuy M, Mekyska J, Font X (2013) A new hand image database simultaneously acquired in visible, near-infrared and thermal spectrums. Cognitive Computation 6.

- <https://doi.org/10.1007/s12559-013-9230-3>, Available at <http://splab.cz/en/download/database/carl-database>
- [31] FLIR (2022) Free flir thermal dataset for algorithm training. Available at <https://www.flir.com/oem/adas/adas-dataset-form/>
- [32] Gade R, Moeslund TB (2018) Constrained multi-target tracking for team sports activities. *IPSN Transactions on Computer Vision and Applications* 10(1):1–11. Available at <https://www.kaggle.com/aalborguniversity/thermal-soccer-dataset>
- [33] Garcia L, Diaz J, Loaiza Correa H, et al (2020) Thermal and visible aerial imagery. <https://doi.org/10.17632/ffgxzx298.2>, Available at <https://data.mendeley.com/datasets/ffgxzx298/2>
- [34] Gebhardt E, Wolf M (2018) Camel dataset for visual and thermal infrared multiple object detection and tracking. In: 2018 15th IEEE International Conference on Advanced Video and Signal Based Surveillance (AVSS), IEEE, pp 1–6, Available at <https://camel.ece.gatech.edu/>
- [35] Ghayoumi zadeh H, Haddadnia J, Seryasat O, et al (2016) Segmenting breast cancerous regions in thermal images using fuzzy active contours <https://doi.org/10.17877/DE290R-17666>, Available at <http://database.irthermo.ir/>
- [36] Ghayoumi zadeh H, Namdari F, Dadpay M, et al (2017) Evaluation of thermal imaging in the diagnosis and classification of varicocele. *Iranian journal of medical physics* 14:114–121. <https://doi.org/10.22038/ijmp.2017.20753.1200>, Available at <http://database.irthermo.ir/>
- [37] Ghiass R, Bendada H, Maldague X (2018) Université laval face motion and time-lapse video database (ul-fmtv). <https://doi.org/10.21611/qirt.2018.051>, Available at <http://www.qirt.org/liens/FMTV.htm>
- [38] Gonzalez Alzate A, Fang Z, Socarras Y, et al (2016) Pedestrian detection at day/night time with visible and fir cameras: A comparison. *Sensors* 16:820. <https://doi.org/10.3390/s16060820>
- [39] HACARUS Inc. (2020) Near infrared hyperspectral image dataset. Available at <https://www.kaggle.com/hacarus/near-infrared-hyperspectral-image>
- [40] HAMAMATSU PHOTONICS K.K., Solid State Division (2011) Characteristics and Use of Infrared Detectors. Tech. rep.
- [41] Haque MA, Bautista RB, Noroozi F, et al (2018) Deep multimodal pain recognition: a database and comparison of spatio-temporal visual modalities. In: 2018 13th IEEE International Conference on Automatic Face & Gesture Recognition (FG 2018), IEEE, pp 250–257, Available at <https://vap.aau.dk/mintpain-database/>
- [42] Huda NU, Hansen BD, Gade R, et al (2020) The effect of a diverse dataset for transfer learning in thermal person detection. *Sensors* 20(7). Available at <https://www.kaggle.com/noorulhuda90/aauptd>
- [43] Hudson R, Hudson J, Levinstein H (1976) Infrared detectors. *Physics Today* 29(3):59
- [44] Hui B, Song Z, Fan H, et al (2019) A dataset for infrared image dim-small aircraft target detection and tracking under ground / air background. <https://doi.org/doi:10.11922/sciencedb.902>, URL <http://www.dx.doi.org/10.11922/sciencedb.902>, Available at <https://www.scidb.cn/en/detail?dataSetId=720626420933459968&dataSetType=journal>
- [45] Hwang S, Park J, Kim N, et al (2015) Multispectral pedestrian detection: Benchmark dataset and baseline. In: Proceedings of the IEEE conference on computer vision and pattern recognition, pp 1037–1045, Available at <https://soonminhwang.github.io/rgbt-ped-detection/>

- [46] Iwashita Y, Nakashima K, Stoica A, et al (2019) Tu-net and tdeeplab: Deep learning-based terrain classification robust to illumination changes, combining visible and thermal imagery. pp 280–285, <https://doi.org/10.1109/MIPR.2019.00057>, Available at [http://robotics.ait.kyushu-u.ac.jp/~yumi/db/jpl\\_marsyard\\_db.html](http://robotics.ait.kyushu-u.ac.jp/~yumi/db/jpl_marsyard_db.html)
- [47] Janani V, Dinakaran M (2014) Infrared image enhancement techniques — a review. In: Second International Conference on Current Trends In Engineering and Technology - ICCTET 2014, pp 167–173, <https://doi.org/10.1109/ICCTET.2014.6966282>
- [48] Karim A, Andersson JY (2013) Infrared detectors: Advances, challenges and new technologies. In: IOP Conference Series: Materials Science and Engineering, IOP Publishing, p 012001
- [49] Kong S, Heo J, Boughorbel F, et al (2007) Multiscale fusion of visible and thermal ir images for illumination-invariant face recognition. *International Journal of Computer Vision* 71:215–233. <https://doi.org/10.1007/s11263-006-6655-0>, Available at <http://vcipl-okstate.org/pbus/bench/>
- [50] Kristan M, Matas J, Leonardis A, et al (2016) A novel performance evaluation methodology for single-target trackers. *IEEE Transactions on Pattern Analysis and Machine Intelligence* 38(11):2137–2155. <https://doi.org/10.1109/TPAMI.2016.2516982>, Available at <https://www.votchallenge.net/vot2019/dataset.html>
- [51] Krišto M, Ivasic-Kos M, Pobar M (2020) Thermal object detection in difficult weather conditions using yolo. *IEEE Access* 8:125,459–125,476. <https://doi.org/10.1109/ACCESS.2020.3007481>, Available at <https://dx.doi.org/10.21227/yec9-yy29>
- [52] Kruse P (1995) A comparison of the limits to the performance of thermal and photon detector imaging arrays. *Infrared Physics & Technology* 36(5):869–882. [https://doi.org/https://doi.org/10.1016/1350-4495\(95\)00014-P](https://doi.org/https://doi.org/10.1016/1350-4495(95)00014-P), URL <https://www.sciencedirect.com/science/article/pii/135044959500014P>
- [53] Kumar A, Srikanth T (2008) Online personal identification in night using multiple face representations. In: 2008 19th International Conference on Pattern Recognition, pp 1–4, <https://doi.org/10.1109/ICPR.2008.4761695>, Available at <https://www4.comp.polyu.edu.hk/~csajaykr/IITD/FaceIR.htm>
- [54] Lee AJ, Cho Y, Shin Ys, et al (2019) Vivid : Vision for visibility dataset. Available at <https://visibilitydataset.github.io/>
- [55] Li SZ, Chu R, Liao S, et al (2007) Illumination invariant face recognition using near-infrared images. *IEEE Transactions on pattern analysis and machine intelligence* 29(4):627–639. Available at <http://vcipl-okstate.org/pbus/bench/>
- [56] Liu H, Bao C, Xie T, et al (2019) Research on the intelligent diagnosis method of the server based on thermal image technology. *Infrared Physics & Technology* 96:390–396. Available at <https://www.kaggle.com/liuhangaz/thermal-images-of-the-server>
- [57] Liu Q, He Z (2018) PTB-TIR: A thermal infrared pedestrian tracking benchmark. CoRR abs/1801.05944. URL <http://arxiv.org/abs/1801.05944>, Available at [https://github.com/QiaoLiuHit/PTB-TIR\\_Evaluation\\_toolkit](https://github.com/QiaoLiuHit/PTB-TIR_Evaluation_toolkit), <https://arxiv.org/abs/1801.05944>
- [58] Liu Q, Li X, He Z, et al (2020) Lsotb-tir: A large-scale high-diversity thermal infrared object tracking benchmark. <https://doi.org/10.1145/3394171.3413922>, Available at <https://github.com/QiaoLiuHit/LSOTB-TIR>
- [59] Lord SD (1992) A new software tool for computing Earth’s atmospheric transmission of near- and far-infrared radiation. NASA Technical Memorandum 103957
- [60] Mantecon T, Del-Blanco C, Jaureguizar F, et al (2016) Hand gesture recognition using infrared imagery provided by leap motion controller. pp 47–57, [https://doi.org/https://doi.org/10.1016/1350-4495\(95\)00014-P](https://doi.org/https://doi.org/10.1016/1350-4495(95)00014-P)

- [org/10.1007/978-3-319-48680-2\\_5](https://doi.org/10.1007/978-3-319-48680-2_5), Available at <https://www.kaggle.com/gti-upm/leapgestrecog>
- [61] Mieziako R (accessed on 2022) Terravic research infrared database. Available at <http://vcipl-okstate.org/pbvs/bench/>
- [62] Miron A (2014) Multi-modal, multi-domain pedestrian detection and classification : Proposals and explorations in visible over stereovision, fir and swir Available at <https://zenodo.org/record/3754168#.YIvye7UzZPa>
- [63] Mohd Asaari MS, Suandi SA, Rosdi B (2014) Fusion of band limited phase only correlation and width centroid contour distance for finger based biometrics. Expert Systems with Applications 41:3367–3382. <https://doi.org/10.1016/j.eswa.2013.11.033>, Available at [http://drfendi.com/fv\\_usm\\_database/](http://drfendi.com/fv_usm_database/)
- [64] Naik S (2019) Thermal mango image dataset - flir one. <https://doi.org/10.17632/vksfkmphzs.1>, Available at <https://data.mendeley.com/datasets/vksfkmphzs/1>
- [65] Najafi M, Baleghi Y, Mirimani SM (2021) Thermal images dataset, transformer, 1 phase dry type. <https://doi.org/10.17632/8mg8mkc7k5.2>, Available at <https://data.mendeley.com/datasets/8mg8mkc7k5/2>
- [66] Nelson J (2020) Thermal dogs and people object detection dataset. Available at <https://public.roboflow.com/object-detection/thermal-dogs-and-people>
- [67] Olmeda D, Premebida C, Nunes U, et al (2013) Pedestrian detection in far infrared images. Integrated Computer-Aided Engineering 20. <https://doi.org/10.3233/ICA-130441>, Available at [https://portal.uc3m.es/portal/page/portal/dpto\\_ing\\_sistemas\\_automatica/investigacion/IntelligentSystemsLab/research/InfraredDataset](https://portal.uc3m.es/portal/page/portal/dpto_ing_sistemas_automatica/investigacion/IntelligentSystemsLab/research/InfraredDataset)
- [68] Palmero C, Clapés A, Holmberg Bahnsen C, et al (2016) Multi-modal rgb-depth-thermal human body segmentation. International Journal of Computer Vision 118. <https://doi.org/10.1007/s11263-016-0901-x>, Available at <https://vap.aau.dk/vap-trimodal-people-segmentation-dataset/>
- [69] Panetta K, Wan Q, Agaian S, et al (2018) A comprehensive database for benchmarking imaging systems. IEEE transactions on pattern analysis and machine intelligence 42(3):509–520. Available at [https://www.kaggle.com/kpvisionlab/tufts-face-database?select=file\\_1](https://www.kaggle.com/kpvisionlab/tufts-face-database?select=file_1)
- [70] Parr AC, Datla R, Gardner J (2005) Optical radiometry, vol 41. Elsevier
- [71] Patino L, Cane T, Vallee A, et al (2016) Pets 2016: Dataset and challenge. In: Proceedings of the IEEE Conference on Computer Vision and Pattern Recognition Workshops, pp 1–8, Available at <http://www.cvg.reading.ac.uk/PETS2016/a.html>
- [72] Piñeiro-Ave J, Blanco-Velasco M, Cruz-Roldán F, et al (2014) Target detection for low cost uncooled mwir cameras based on empirical mode decomposition. Infrared Physics & Technology 63:222–231
- [73] Portmann J, Lynen S, Chli M, et al (2014) People detection and tracking from aerial thermal views. In: 2014 IEEE International Conference on Robotics and Automation (ICRA), pp 1794–1800, <https://doi.org/10.1109/ICRA.2014.6907094>, Available at <https://projects.asl.ethz.ch/datasets/doku.php?id=ir%3Airicra2014>
- [74] Prasad DK, Rajan D, Rachmawati L, et al (2017) Video processing from electro-optical sensors for object detection and tracking in a maritime environment: A survey. IEEE Transactions on Intelligent Transportation Systems 18(8):1993–2016. <https://doi.org/10.1109/TITS.2016.2634580>, Available at <https://sites.google.com/site/dilipprasad/home/singapore-maritime-dataset>
- [75] Roboflow (2020) Thermal cheetah object detection dataset. Available at <https://public.roboflow.com/object-detection/>

*thermal-cheetah*

- [76] Rogalski A (1997) Infrared thermal detectors versus photon detectors: I. Pixel performance. In: Sizov FF, Tetyorkin VV (eds) *Material Science and Material Properties for Infrared Optoelectronics*, International Society for Optics and Photonics, vol 3182. SPIE, pp 14–25, URL <https://doi.org/10.1117/12.280417>
- [77] Rogalski A (2002) Infrared detectors: an overview. *Infrared physics & technology* 43(3-5):187–210
- [78] Sedik A, Abd El-Rahiem B, Abd El-Samie F, et al (2020) Mbd: Multi-biometric dataset. <https://doi.org/10.17632/94ksjgbwnz.1>, Available at <https://data.mendeley.com/datasets/94ksjgbwnz/1>
- [79] SENSIAC (2008) Military sensing information analysis center (sensiacy). Available at [https://www.sensiacy.org/external/products/list\\_databases/](https://www.sensiacy.org/external/products/list_databases/)
- [80] Shahroudy A, Liu J, Ng TT, et al (2016) Ntu rgb+d: A large scale dataset for 3d human activity analysis. In: *Proceedings of the IEEE conference on computer vision and pattern recognition*, pp 1010–1019, Available at <https://rose1.ntu.edu.sg/dataset/actionRecognition/>
- [81] Shamsoshoara A, Afghah F, Razi A, et al (2021) Aerial imagery pile burn detection using deep learning: The flame dataset. *Computer Networks* 193:108,001. <https://doi.org/10.1016/j.comnet.2021.108001>, Available at <https://dx.doi.org/10.21227/qad6-r683>
- [82] Silva A, Calado C (2020) Thermal and optical behavior dataset of surfaces coated with high reflectance and common materials under different conditions, used in brazil. *Data in Brief* 30:105,445. <https://doi.org/10.1016/j.dib.2020.105445>, Available at <https://data.mendeley.com/datasets/gnhjwsf6jf/2>
- [83] Socarras Y, Ramos S, Vazquez D, et al (2013) Adapting pedestrian detection from synthetic to far infrared images. Available at <http://adas.cvc.uab.es/elektra/enigma-portfolio/>

*item-1/*

- [84] Sousa E, Vardasca R, Teixeira S, et al (2017) A review on the application of medical infrared thermal imaging in hands. *Infrared Physics & Technology* 85:315–323. <https://doi.org/https://doi.org/10.1016/j.infrared.2017.07.020>, URL <https://www.sciencedirect.com/science/article/pii/S1350449517304024>
- [85] Speth J, Vance N, Czajka A, et al (2021) Deception detection and remote physiological monitoring: A dataset and baseline experimental results Available at <https://cvgl.nd.edu/projects/data/>
- [86] Strat T (2005) Vivid tracking evaluation web site. Available at <http://vision.cse.psu.edu/data/vividEval/datasets/datasets.html>
- [87] Strohmayer J, Pramerdorfer C, Kampel M (2020) Sdt: A synthetic multi-modal dataset for person detection and pose classification Available at <https://zenodo.org/record/4124309#.YWIgKRpBxPZ>
- [88] Sun X, Guo L, Zhang W, et al (2021) A dataset for small infrared moving target detection under clutter background. v1. Available at <https://datapid.cn/31253.11.sciencedb.j00001.00231>
- [89] Toet A (2002) Detection of dim point targets in cluttered maritime backgrounds through multisensor image fusion. In: *Targets and Backgrounds VIII: Characterization and Representation*, International Society for Optics and Photonics, pp 118–129, Available at [https://figshare.com/articles/dataset/Kayak\\_image\\_fusion\\_sequence\\_Part\\_I/1007650](https://figshare.com/articles/dataset/Kayak_image_fusion_sequence_Part_I/1007650)
- [90] Toet A, Hogervorst MA, Pinkus AR (2016) The triclobs dynamic multi-band image dataset. Available at [https://figshare.com/articles/dataset/The\\_TRICLOBS\\_Dynamic\\_Multiband\\_Image\\_Dataset/3206887/1](https://figshare.com/articles/dataset/The_TRICLOBS_Dynamic_Multiband_Image_Dataset/3206887/1)
- [91] Tu Z, Ma Y, Li Z, et al (2020) Rgbt salient object detection: A large-scale dataset and



- benchmark. arXiv preprint arXiv:200703262 Available at <https://github.com/lz118/RGBT-Salient-Object-Detection>
- [92] Venkataraman B, Raj B (2003) Performance parameters for thermal imaging systems. *Insight-Non-Destructive Testing and Condition Monitoring* 45(8):531–535
- [93] Visual Lab. (accessed on 2022) Thermal images for breast cancer diagnosis dmr-ir. Available at <http://visual.ic.uff.br/en/proeng/thiagoelias/>
- [94] Vollmer M, Möllmann KP (2017) Infrared thermal imaging: fundamentals, research and applications. John Wiley & Sons
- [95] Wang Y, Jodoin PM, Porikli F, et al (2014) Cdnet 2014: An expanded change detection benchmark dataset. In: *Proceedings of the IEEE conference on computer vision and pattern recognition workshops*, pp 387–394, Available at <http://jacarini.dinf.usherbrooke.ca/dataset2014/>
- [96] Wayne Treible SSAKMOBPKSCK-Philip Saponaro (2017) Cats: A color and thermal stereo benchmark. In: *Conference on Computer Vision and Pattern Recognition (CVPR)*, Available at <http://bigdatavision.org/CATS/download.html>
- [97] Westlake ST, Volonakis TN, Jackman J, et al (2020) Deep learning for automatic target recognition with real and synthetic infrared maritime imagery. In: *Artificial Intelligence and Machine Learning in Defense Applications II*, International Society for Optics and Photonics, p 1154309, Available at <https://cord.cranfield.ac.uk/articles/dataset/IRShips/12800324>
- [98] Wu Z, Fuller N, Theriault D, et al (2014) A thermal infrared video benchmark for visual analysis. In: *2014 IEEE Conference on Computer Vision and Pattern Recognition Workshops*, pp 201–208, <https://doi.org/10.1109/CVPRW.2014.39>, Available at <http://csr.bu.edu/BU-TIV/BUTIV.html>
- [99] Xiang S (2020) Spindle thermal error prediction approach based on thermal infrared images: a deep learning method. <https://doi.org/10.21227/vwp1-q708>, Available at <https://dx.doi.org/10.21227/vwp1-q708>
- [100] Xu Z, Zhuang J, Liu Q, et al (2019) Benchmarking a large-scale fir dataset for on-road pedestrian detection. *Infrared Physics & Technology* 96:199–208. <https://doi.org/10.1016/j.infrared.2018.11.007>
- [101] Yaman M, Kalkan S (2015) An iterative adaptive multi-modal stereo-vision method using mutual information Available at <https://kovan.ceng.metu.edu.tr/MMStereoDataset/>
- [102] Yoon JS, Park K, Hwang S, et al (2016) Thermal-infrared based drivable region detection. In: *Intelligent Vehicles Symposium (IV)*, 2016 IEEE, IEEE, pp 978–985, Available at <https://sites.google.com/site/drivableregion/>
- [103] Zhang H, Luo C, Wang Q, et al (2018) A novel infrared video surveillance system using deep learning based techniques. *Multimedia Tools and Applications* 77(20):26,657–26,676. Available at <http://www.lpi.tel.uva.es/AALARTDATA>
- [104] Zhang L, Rui Y (2013) Image search—from thousands to billions in 20 years. *ACM Trans Multimedia Comput Commun Appl* 9(1s). <https://doi.org/10.1145/2490823>, URL <https://doi.org/10.1145/2490823>
- [105] Zhang MM, Choi J, Daniilidis K, et al (2015) Vais: A dataset for recognizing maritime imagery in the visible and infrared spectrums. In: *2015 IEEE Conference on Computer Vision and Pattern Recognition Workshops (CVPRW)*, pp 10–16, <https://doi.org/10.1109/CVPRW.2015.7301291>, Available at <http://vcip1-okstate.org/pbvs/bench/>
- [106] Zukal M, Mekyska J, Cika P, et al (2013) Interest points as a focus measure in multi-spectral imaging. *Radioengineering* 22:68–81. Available at <http://splab.cz/en/download/databaze/multispec>